An Optimal Burn Regime in a Controlled Tokamak Fusion Power Plant

Julio J. Martinell and Javier E. Vitela

***Abstract*— The optimal conditions for the burn regimes of a tokamak fusion power plant are obtained under the assumption that electron and ion temperatures can be controlled independently by means of external auxiliary heating. The study of the system is based on a volume-averaged 0-D two-temperature model in which different operating states are obtained by proper adjustment of the deuterium-tritium refueling rate and the auxiliary heating power to electrons and to ions. Optimal operating conditions that maximize Q power gain are determined using plasma operation contour plots. For the H-mode, the optimal burn regimes for a given fusion power are shown to be obtained when the auxiliary heating power to the plasma ions vanishes. The impact on the optimal operating states of varying the enhancement factor of the energy confinement time is found to be important. Impurities composed of beryllium and argon are included in two different scenarios that give similar results. An ideal system free of impurities is also presented to show that a clean plasma would significantly improve its performance.**

***Index Terms*— Fusion reactors, plasma confinement, tokamak.**

I. Introduction

IN ORDER to optimize the performance of a fusion power plant, it is necessary to minimize the auxiliary heating requirements. The ultimate goal is to achieve the ignition state where no auxiliary heating is required. Then, most of the heating of a burning plasma should be due to fusion reactions, which in a deuterium-tritium (DT) fueled tokamak reactor heat the plasma through the energetic alpha particles that are created. They deposit most of their energy into the electrons, with only a small fraction going to the plasma ions. Thus, electron temperature will be higher and the reactor will operate in the hot electron mode. To describe this situation, it is necessary to analyze the operation of a fusion reactor by considering two different temperatures for ions and electrons.

In contrast to other studies in which a one-temperature model was used [1]–[5], in this paper, we analyze burning regimes of a two-temperature plasma in a tokamak device. For definiteness, the design parameters of International Thermonuclear Experimental Reactor (ITER) [6] are used, but the analysis could be applied to any other system. To keep it simple, we use a 0-D model in which energy transport is accounted for by a global energy confinement time τ_E taken from the IPB98(y, 2) scaling. Deuterium and tritium particle transport as well as helium ash accumulation is also accounted for by means of global confinement times assuming $\tau_p, \tau_{He} \propto \tau_E$. Different operating conditions can be obtained by appropriately adjusting the DT refueling rate and the independent auxiliary heating to electrons and to ions. Here, plasma operation contour (POPCON) diagrams [7] are used to identify the optimal operating conditions, i.e., those states that maximize the Q-gain for a given fusion power level. The operating points studied in this work are constrained to keep a fixed electron-to-ion temperature ratio $T_i/T_e =$ constant (although $(T_e - T_i) =$ constant was also studied). This means that going from one steady state to another, while seeking to attain the optimal one, the electron temperature and density are varied independently, but the ion temperature is determined by the fixed relation. This can be achieved by tailoring auxiliary heating to each species appropriately. We focus the attention on the hot electron mode ($T_e > T_i$) since this is the one expected for the operation of a subignited burning plasma. A similar analysis has been used to study the thermal stability of a fusion power plant [8], [9].

Our aim in this paper is to show that the optimal operating states of a reactor can be attained for zero external heating to the ions. We are not concerned about how to go from one state to another, but we assume that it is always possible to reach the desired state by controlling the external parameters like the auxiliary heating and the refueling rate. Another control parameter is the helium content, which could be extracted or injected as needed. The operating states are thus characterized by the electron temperature and density, which in turn determine all other relevant quantities. This is an attractive operation option since the power requirements are reduced by turning off external ion heating such as ion cyclotron range of frequencies (ICRF) heating maintaining just electron external heating, like electron cyclotron resonant heating (ECRH). Since we also assume H-mode operation, it is of interest to mention that ECRH can also be used to produce transport barriers leading to H-mode [10]. We first study with some details the case for which the ion to electron temperature ratio T_i/T_e is constant, and then compare with some cases that use the alternative condition that keeps $T_e - T_i$ constant. The results are qualitatively the same indicating that the fundamental conclusions do not depend on the actual temperature relation.

This paper considers that the plasma contains impurities composed of a light element, beryllium, and a heavy element, argon, and analyze the cases when the number density of Ar is fixed and when the fractional density n_{Ar}/n_e is kept constant.

Manuscript received March 26, 2015; accepted January 24, 2016. Date of publication February 12, 2016; date of current version March 8, 2016. This work was supported in part by the DGAPA Project, Universidad Nacional Autónoma de México under Grant IN109115 and in part by the Consejo Nacional de Ciencia y Tecnología under Grant 152905.

J. J. Martinell is with the Instituto de Ciencias Nucleares, Universidad Nacional Autónoma de México, Mexico City 04510, Mexico (e-mail: martinel@nucleares.unam.mx).

Javier E. Vitela, deceased, was with the Instituto de Ciencias Nucleares, Universidad Nacional Autónoma de México, Mexico City 04510, Mexico (e-mail: vitela@nucleares.unam.mx).

Color versions of one or more of the figures in this paper are available online at http://ieeexplore.ieee.org.

Digital Object Identifier 10.1109/TPS.2016.2521884

In both of these cases, the beryllium fractional density is assumed to be fixed. As a reference case, we also study the ideal situation in which no impurities are present.

This paper is divided as follows. In Section II, we discuss the physical model used in this paper. Section III presents the results for steady-state operation using POPCON plots. The results of the case where the beryllium fractional density $f_{\rm Be}$ and the argon particle density $n_{\rm Ar}$ are fixed are presented in Section III-A; in addition, the results and discussions of the optimal conditions for maximum energy gain are given and the dependence of the optimal operating conditions on the energy confinement time values is shown. In Section III-B, the alternative case where both fractional densities $f_{\rm Be}$ and $f_{\rm Ar}$ are fixed is analyzed. Section III-C presents some results for the ideal case where no impurities are present and Section III-D studies the effect of modifying some electron/ion relationships. Finally, in Section IV, the main results are discussed and conclusions are drawn.

II. Physical Model

The equations that govern particle balance (ions and alphas) and energy density balance (electrons and ions) are

$$\frac{\partial}{\partial t}n_{\rm DT} = S_f - \frac{1}{2}n_{\rm DT}^2\langle\sigma\upsilon\rangle - \nabla\cdot\vec{\Gamma}_{\rm DT} \tag{1}$$

$$\frac{\partial}{\partial t}n_\alpha = \frac{1}{4}(1-f_{\rm frac})n_{\rm DT}^2\langle\sigma\upsilon\rangle - \nabla\cdot\vec{\Gamma}_\alpha \tag{2}$$

$$\begin{aligned}\frac{\partial}{\partial t}\left[\frac{3}{2}n_eT_e\right] &= \mathcal{P}_{{\rm aux},e} + \frac{1-f_{\rm frac}}{4}f_eQ_\alpha n_{\rm DT}^2\langle\sigma\upsilon\rangle \\ &\quad + \mathcal{P}_{\rm oh} - A_bZ_{\rm eff}n_e^2T_e^{1/2} - \frac{3}{2}n_e\frac{T_e-T_i}{\tau_{\rm ei}} \\ &\quad - \mathcal{P}_{\rm cycl} - \nabla\cdot\vec{q}e\end{aligned} \tag{3}$$

and

$$\begin{aligned}&\frac{\partial}{\partial t}\left[\frac{3}{2}(n_{\rm DT}+n_\alpha+n_{\rm Be}+n_{\rm Ar})T_i\right] \\ &= \mathcal{P}_{{\rm aux},i} + \frac{1-f_{\rm frac}}{4}f_i\,Q_\alpha n_{\rm DT}^2\langle\sigma\upsilon\rangle + \frac{3}{2}n_e\frac{T_e-T_i}{\tau_{\rm ei}} - \nabla\cdot\vec{q}_i.\end{aligned} \tag{4}$$

The quantities $\vec{\Gamma}_{\rm DT}$ and $\vec{\Gamma}_\alpha$ and $\vec{q}_e$ and $\vec{q}_i$ are the DT and alpha particle fluxes and the electron and ion energy fluxes due to transport, respectively. Energy losses include bremsstrahlung [11] and cyclotron radiation $\mathcal{P}_{\rm cycl}$ [12]. The coefficient A_b corresponds to the bremsstrahlung radiation losses and $\mathcal{P}_{\rm oh} = \mathbf{E}\cdot\mathbf{j}$ is the ohmic heating, which is assumed to be solely due to the induced plasma current I (bootstrap and current drive are considered to be absent or small) and thus approximated by $\eta(I/A)^2$, with η being the neoclassical resistivity [13] and A the cross sectional area. The effective charge $Z_{\rm eff}$ is given by

$$Z_{\rm eff} = \frac{\sum_{\rm ions}Z_i^2n_i}{\sum_{\rm ions}Z_in_i}. \tag{5}$$

$\tau_{\rm ei}$ is the relaxation time for electron–ion energy equipartition and $\langle\sigma\upsilon\rangle$ is the DT reactivity given by the expression [14]

$$\langle\sigma\upsilon\rangle = c_1\theta\sqrt{\xi/\left(m_rc^2T_i^3\right)}\exp\left(-3\xi\right) \tag{6}$$

with

$$\xi = \left[B_g^2/(4\theta)\right]^{1/3}$$

and

$$\theta = T_i\Big/\left[1-\frac{T_i(c_2+T_i(c_4+c_6T_i))}{1+T_i(c_3+T_i(c_5+c_7T_i))}\right] \tag{7}$$

where $T_i = T_i(r,t)$ is the local ion temperature in kiloelectronvolts. The values of the parameters m_rc^2, B_g, and $c_1,\ldots,c_7$ can be found in [14]. Thermalization of the alpha particles produced by fusion is assumed to be instantaneous. The birth energy of the alpha particles is $Q_\alpha = 3.5$ MeV, $f_{\rm frac}$ is the effective fraction of alpha particles that are anomalously lost due to MHD events before they are thermalized, and f_e and f_i are the fractions of the alpha particle energy Q_α deposited into the electrons and ions, respectively. We will assume that the impurities are solely composed of Be and Ar. Thus, the quasi-neutrality condition is $n_e = n_{\rm DT} + 2n_\alpha + Z_{\rm Be}n_{\rm Be} + Z_{\rm Ar}n_{\rm Ar}$, where n_e is the electron number density.

The 0-D equations are obtained from the volume average of the above equations. For the optimization analysis we make here, the shape of the radial profiles is unimportant since stability and transport phenomena are not involved. Thus, for simplicity, we assume flat particle density profiles $n_k(r) = n_k^0$ ($k = e, {\rm DT}, \alpha$, Be, Ar) and temperature radial profiles for both electrons and ions of the form [15]

$$T_k(\vec{r},t) = T_k^0(t)[1-\psi/\psi_0]^{\gamma_t} \tag{8}$$

with T_k^0 ($k = e,i$) being the central temperature and ψ the toroidal magnetic flux coordinate, and ψ_0 the total flux enclosed at the tokamak boundary.

The volume average of (1)–(4) gives a set of coupled nonlinear differential equations for the evolution of $n_{\rm DT}$, the helium ash n_α, and the peak electron and ion temperatures T_e^0 and T_i^0. Because of a lack of proper understanding concerning particles and energy plasma transport, volume average transport losses are usually taken into account in 0-D studies through the energy confinement times of the electrons and the ions $\tau_{E,e}$ and $\tau_{E,i}$, as well as by the DT and the helium ash confinement times τ_p and τ_α, respectively. The resulting equations take the form

$$\frac{d}{dt}n_{\rm DT} = \langle S_f\rangle_v - \frac{1}{2}n_{\rm DT}^2\langle\sigma\upsilon\rangle_v - n_{\rm DT}/\tau_p \tag{9}$$

$$\frac{d}{dt}n_\alpha = \frac{1}{4}(1-f_{\rm frac})n_{\rm DT}^2\langle\sigma\upsilon\rangle_v - n_\alpha/\tau_\alpha \tag{10}$$

$$\begin{aligned}\frac{d}{dt}\frac{3}{2}n_e\langle T_e\rangle_v &= \langle\mathcal{P}_{{\rm aux},e}\rangle_v + \frac{1-f_{\rm frac}}{4}\,fe\,Q_\alpha n_{\rm DT}^2\langle\sigma\upsilon\rangle_v \\ &\quad + A_hZ_{\rm eff}^{1/2}\left(\frac{1+1.198Z_{\rm eff}^{1/2}+0.222Z_{\rm eff}}{1+2.966Z_{\rm eff}^{1/2}+0.75Z_{\rm eff}}\right) \\ &\quad \times\frac{F_{\rm ohm}}{T_e^{3/2}}\left(1+\frac{3\gamma_t}{2}\right) - \frac{A_{\rm cyc}}{1+\frac{5\gamma_T}{2}}n_e^{1/2}T_e^{2.5} \\ &\quad \times\frac{1+\frac{1.9303}{511}T_e}{1-\frac{0.58167}{511}T_e}\left(1+\frac{18a}{RT_e^{0.5}}\right)^{0.5} \\ &\quad - A_bZ_{\rm eff}F_{\rm rad}\frac{n_e^2}{1+\gamma_t/2}T_e^{1/2} \\ &\quad - \left(\frac{1+3\gamma_t/2}{1+\gamma_t}\right)\frac{3}{2}n_e\frac{T_e-T_i}{\tau_{\rm ei}} \\ &\quad - \left(\frac{1}{1+\gamma_t}\right)\frac{3}{2}n_e\frac{T_e}{\tau_{E,e}}\end{aligned} \tag{11}$$

and

$$\frac{d}{dt}\left[\frac{3}{2}(n_{\rm DT}+n_\alpha+n_{\rm Be}+n_{\rm Ar})\langle T_i\rangle_v\right] = \langle \mathcal{P}_{{\rm aux},i}\rangle_v + \frac{1}{4}(1-f_{\rm frac})f_i Q_\alpha n_{\rm DT}^2\langle\sigma v\rangle_v + \left(\frac{1+\frac{3\gamma_t}{2}}{1+\gamma_t}\right)\frac{3}{2}n_e\frac{T_e-T_i}{\tau_{\rm ei}} - \left(\frac{1}{1+\gamma_t}\right)\frac{3}{2}(n_{\rm DT}+n_\alpha+n_{\rm Be}+n_{\rm Ar})\frac{T_i}{\tau_{E,i}} \quad (12)$$

where the electron–ion relaxation time $\tau_{\rm ei}$ is given by the expression [16]

$$\tau_{\rm ei} = \frac{3}{8\sqrt{2\pi}m_e^{1/2}e^4\ln\Lambda_e}\frac{T_e^{3/2}}{\sum_{\rm ions}Z_i^2 n_i/m_i}. \quad (13)$$

In these equations, for simplicity, we have removed the superscript 0 in the electron and ion central temperature notation, and thus *from now on*, T_i and T_e will denote the *central* temperatures.

In order to include the contribution of line radiation losses, in (11), we have included the fudge factor $F_{\rm rad} = 2$ such that the bremsstrahlung losses in this model match the design values of the combined bremsstrahlung and line radiated power at the reference values of the electron and ion temperatures and particle density reported for ITER. For the same reason, we have also included the fudge factor $F_{\rm ohm} = 1.85$ in the ohmic heating term, which accounts for differences in the profile averaging procedure, in order to give the design power of 1 MW at the nominal operating point. The constant $A_{\rm cyc}$ is given in [12] and for our parameters equals 1.23×10^{-15} MW/m^3, while $A_h = 0.0324$ MW/m^3 and $A_b = 5.327\times10^{-43}$ MW/m^3 when T_e and n are in kiloelectronvolts and particles per cubic meter, respectively.

The volume average of the DT reactivity $\langle\sigma v\rangle_v$ used in the above equations can be written as

$$\langle\sigma v\rangle_v = G(\gamma_t, T_i)\times\langle\sigma v\rangle \quad (14)$$

where G is a correction factor for the radial profile in (8), which is given by

$$G(\gamma_t,T_i) = 0.249 + 0.017T_i - 0.00011T_i^2 - 0.13\gamma_t + 0.023\gamma_t^2 - 0.00769\gamma_t T_i + 0.000067T_i^2\gamma_t + 0.00125T_i\gamma_t^2 - 0.0000126T_i^2\gamma_t^2 \quad (15)$$

where T_i is the central ion temperature in kiloelectronvolts and $\langle\sigma v\rangle$ is the expression for the reactivity in (6) evaluated at the central ion temperature.

The energy confinement time τ_E will be estimated using the IPB98(y, 2) scaling [6], [20]

$$\tau_{\rm IPB98}(y,2) = 0.0562HI^{0.93}R^{1.97}B^{0.15}M_{\rm eff}^{0.19}\epsilon^{0.58}\kappa^{0.78}n_e^{0.41}P_s^{-0.69} \quad (16)$$

where the factor H expresses the degree of enhancement expected over the current mean prediction. The values of the parameters in (16) were taken from the values reported for ITER [6]. First, the simplifying assumption $\tau_{E,i} = \tau_{E,e} = \tau_E$ is used, which means that ion and electron channels have the same scaling, an assertion that is supported by studies based on experimental data from different machines made in [18]. They find that in H-mode, $\tau_{E,i}$ and $\tau_{E,e}$ are consistent with the gyro-Bohm scaling, which in turn agrees with the global τ_E given by (16) [18]. The actual values of $\tau_{E,i}$ and $\tau_{E,e}$ may be different, so we allow a variation of the ratio $\zeta = \tau_{E,i}/\tau_{E,e}$.

Although the scaling (16) has been obtained from past and current devices that operate in the hot ion mode, some recent results have shown that the energy confinement time does not depend on either the electron to ion temperatures ratio T_e/T_i or the electron to ion input power ratio; only the total net heating power is involved in τ_E [17]. It has been argued [18] that the observed dependence of the thermal diffusivity on T_e/T_i would lead to a corresponding dependence of τ_E on T_e/T_i, but in [17], it is shown that there is also a temperature gradient change when T_e/T_i is modified that compensates for the diffusivity, making τ_E independent of T_e/T_i. Thus, up to date, there is no evidence of any modification required to the above scaling for the hot electron mode expected for a reactor.

The gain factor Q_G, defined as the ratio of the energy generation rate in the plasma due to the fusion reactions to the total external heating power, measures how close a fusion reactor is to ignition conditions

$$Q_G = \frac{\langle\mathcal{P}_{\rm fusion}\rangle_v}{\langle\mathcal{P}_{\rm aux}+\mathcal{P}_{\rm ohmic}\rangle_v} \quad (17)$$

where $\mathcal{P}_{\rm aux}$ includes both the auxiliary heating to electrons and to ions and $\mathcal{P}_{\rm fusion}$ takes into account the total energy produced in the DT fusion reactions, i.e., the energy carried by the alpha particles and by the neutrons. When $\zeta = \tau_{E,i}/\tau_{E,e} \neq 1$, the resulting values of Q_G and other quantities are modified, but the main relationships are maintained.

Important empirical quantities to be considered are the L-H mode transition power threshold M

$$M = P_s/P_{\rm thresh} \quad (18)$$

with [19]

$$P_{\rm thresh} = 4.30M_{\rm eff}^{-1}B^{0.772}n_e^{0.782}R^{0.999}a^{0.975} \quad (19)$$

and the Greenwald density limit

$$n_G = I/(\pi a^2). \quad (20)$$

It is required that M must be larger than one for H-mode operation [15], [20]. In these equations, $P_{\rm thresh}$ and P_s are in megawatts. On the other hand, n_G is an empirical upper density limit to avoid plasma disruptions and confinement degradation when operating near this limit. However, it has been found that operation of tokamaks at higher densities is possible under certain conditions [21]–[23]. In (16) and (18), $P_s = (\mathcal{P}_\alpha+\mathcal{P}_{{\rm aux},e}+\mathcal{P}_{{\rm aux},i}+\mathcal{P}_{\rm ohm}-\mathcal{P}_{\rm rad})\times V_{\rm core}$, with $V_{\rm core}$ the volume of the plasma; n_e is the electron density normalized to 10^{19} m^{-3} in (16), while it is normalized to 10^{20} m^{-3} in (19) and (20); and B is in Teslas, R and a are in meters, and the current I is in megaamperes.

During the thermalization of the α particles produced by fusion, they are in the energy range between 3.5 MeV and the volume average plasma nominal temperature ~8 keV, and in this range, the velocity of the alpha particles is greater than

the thermal velocity $\sqrt{2T/m_i}$ of the ions and much smaller than the thermal velocity of the electrons. In this interval ($v_{\mathrm{th},i} \ll v_\alpha \ll v_{\mathrm{th},e}$), the rate of energy loss of the alpha particles is approximately given by [24]–[26]

$$-\frac{d}{dt}E_\alpha = \frac{32\sqrt{\pi}\,Z_\alpha^2 e^4 n_e}{3m_e m_\alpha}\frac{\ln\Lambda_e}{v_{\mathrm{th},e}^3}E_\alpha + \sum_{\mathrm{ions}}\frac{4\pi\,Z_\alpha^2 Z_i^2 e^4 n_i}{\sqrt{2m_\alpha}}\left(1+\frac{m_\alpha}{m_i}\right)\frac{\ln\Lambda_i}{E_\alpha^{1/2}} \quad (21)$$

where the first term on the right-hand side is the energy absorbed by the plasma electrons and the last term is the energy lost to the ions. Thus, above a certain energy value, the alpha particles lose their energy mainly to the electrons. This critical energy is given by

$$E_{\mathrm{crit}} = \frac{m_\alpha v_{\mathrm{th},e}^2}{2}\left[\frac{3\sqrt{\pi}}{4}\frac{m_e}{m_\alpha}\sum_{\mathrm{ions}}\frac{\ln\Lambda_i}{\ln\Lambda_e}\left(1+\frac{m_\alpha}{m_i}\right)Z_i^2\frac{n_i}{n_e}\right]^{2/3}. \quad (22)$$

Using (21) to determine the energy deposited into electrons and ions during thermalization, we find that approximately 85% of the energy of the fusion alphas is absorbed by the electrons and only 15% by the ions.

The reference operating state for the studies presented in the following is $n_0 = 10^{20}$ m^{-3}, and $T_{e0} = 23.6$ keV and $T_{i0} = 23.0$ keV for the electron density and the peak temperatures of the electrons and the ions, respectively. The radial profile parameter γ_t will be taken to be equal to 1.85 for both electron and ion temperatures. It will be assumed that 10% of the alpha particles produced are anomalously lost before they are thermalized, and hence, we take $f_{\mathrm{frac}} = 0.1$. Following the previous discussion, we assume $f_e = 0.85$ and $f_i = 0.15$. Similarly to other studies, we take into account the effect of helium ash accumulation self-consistently assuming $\tau_\alpha = 6.8\tau_E$, and likewise for the global transport losses of DT, we take $\tau_{\mathrm{DT}} = \tau_\alpha$. The ionization charges for the impurity ions will be taken as $Z_{\mathrm{Ar}} = 17$ and $Z_{\mathrm{Be}} = 4$. The Greenwald density limit n_G is 1.194, which corresponds to a horizontal line in the POPCON plots shown in the following at $n_e/n_{e0} = 1.19$.

Equations (9)–(12) are solved for *steady state* ($\partial/\partial t = 0$) scanning over density and electron temperature around the reference state, in order to generate POPCON plots. The corresponding ion temperature is determined from the constant ratio $T_i/T_e = 0.975$, obtained from the reference values of T_{e0} and T_{i0}. For each (n_e, T_e) value, the solution of the four equations gives the values of the four quantities: DT refueling rate S_{DT}, fractional density of helium ash f_α, and the auxiliary heating power to electrons $P_{\mathrm{aux},e}$ and the auxiliary heating power to ions $P_{\mathrm{aux},i}$. By fixing a temperature ratio lower than one, we are constrained to operation in the hot electron mode.

III. Characterization of Operational States

The impurity content determines the properties of the operational states. Here, we keep f_{Be} constant at 0.02 and for argon, two cases are considered: constant n_{Ar} and constant f_{Ar}.

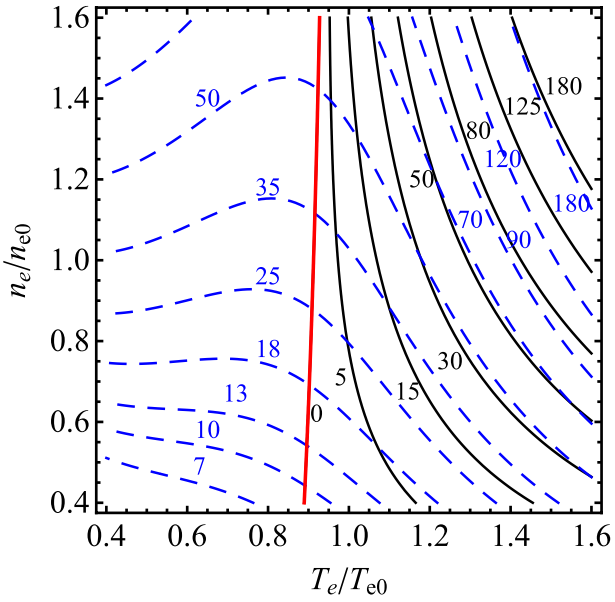

Fig. 1. Contour plot in the normalized T_e–n_e space of auxiliary heating power to electrons (dashed lines) and auxiliary heating to ions (solid lines) in megawatts, for constants f_{Be} and n_{Ar} with $H = 1$. Red line: $P_{\mathrm{aux},i} = 0$.

A. Case f_{Be} and n_{Ar} Constant

Here, we analyze the results when the density of Ar is fixed at $n_{\mathrm{Ar}} = 1.2 \times 10^{17}$ m^{-3} for all operating points. Figs. 1–5 show POPCON plots summarizing the results obtained with an enhancement factor $H = 1$ in the energy scaling law in (16). In Fig. 1, we show the contour plots of the auxiliary heating power to electrons and ions. We found that for a constant electron density, the auxiliary heating power to the ions decreases when the operational electron temperature decreases reaching a point where $P_{\mathrm{aux},i} = 0$. Note that in Fig. 1, we did not include contour lines with $P_{\mathrm{aux},i} < 0$ because these states are not physically plausible under the steady-state conditions considered here. These states are unstable since, given the fact that $P_{\mathrm{aux},i}$ cannot be negative, making $P_{\mathrm{aux},i} = 0$ in (12) (keeping all the other terms at their steady-state values) would imply a positive time derivative. Thus, the line $P_{\mathrm{aux},i} = 0$ represents a cutoff for the available operating points of the reactor, where they are marginally stable.

In Fig. 2, the contour lines of the gain factor Q_G as obtained from (17) are shown. In Fig. 2, we also show the states of constant total fusion power, which include the energy of the neutrons produced by the fusion reactions. In addition, Fig. 2 includes the boundary line for which $P_{\mathrm{aux},i} = 0$. We observe that for a fixed fusion power value, we can decrease the electron temperature by simultaneously increasing the electron density, properly moving along the corresponding $P_{\mathrm{fusion}} =$ constant line, thus increasing the Q_G monotonically until the boundary $P_{\mathrm{aux},i} = 0$ is reached. For instance, at the reference operating point (T_{e0}, n_{e0}), which is the point (1, 1) in the normalized space of the POPCON plots, the total fusion power is 489 MW with a gain of $Q_G = 11.5$. The operation at this state requires $P_{\mathrm{aux},e} = 33.7$ MW auxiliary power to the electrons and $P_{\mathrm{aux},i} = 7.6$ MW auxiliary heating power to

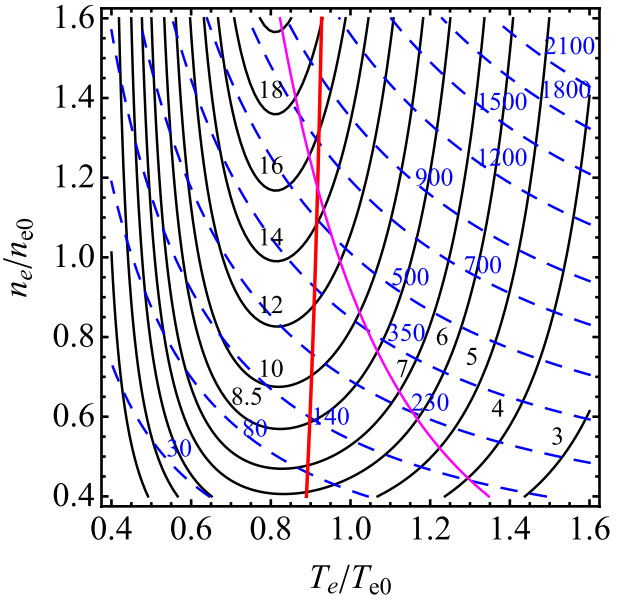

Fig. 2. Contours of total fusion power in megawatts (dashed lines) and the Q_G factor (solid lines), for constant f_{Be} and n_{Ar} with $H = 1$. Red line: $P_{\mathrm{aux},i} = 0$. Magenta line: L-H transition threshold $M = 1$.

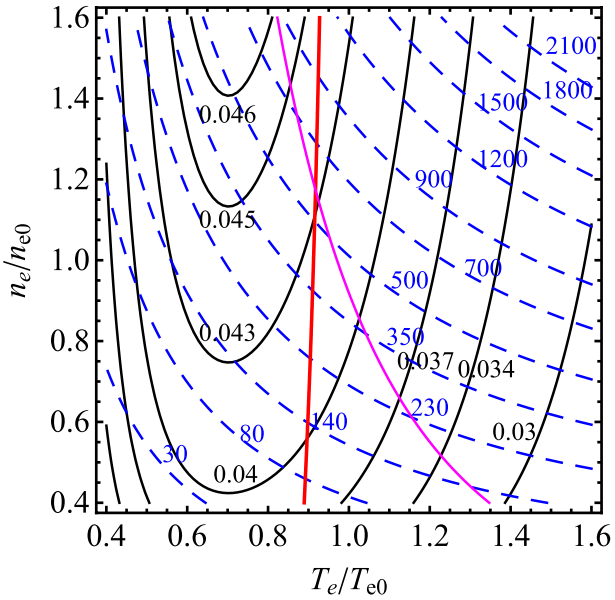

Fig. 3. Case f_{Be} and n_{Ar} constant with $H = 1$. Contours of the fraction of helium ash n_α/n_e (solid lines) and total fusion power (dashed lines). Boundaries of zero auxiliary heating power to ions and the L-H transition limit are shown.

the plasma ions; the bremsstrahlung and cyclotron radiation losses at this point are $P_{\mathrm{b}} = 37.7$ MW and $P_{\mathrm{cyc}} = 8.2$ MW, respectively. Thus, from Fig. 2, we see that while maintaining the same fusion power, it is possible to increase the gain up to $Q_G \approx 14$ by decreasing the electron temperature to 0.9 T_{e0} and increasing the electron density to the value 1.16 n_{e0}. At this new operation point, there is no auxiliary heating to the ions, while the auxiliary heating to the electrons increases only slightly to around 36 MW.

In general, the intersection of the boundary line $P_{\mathrm{aux},i} = 0$ with the contour line corresponding to $P_{\mathrm{fusion}} =$ constant in the n_e–T_e space gives the operational state for which Q_G is maximum for that particular fusion power. Trying to get to higher Q_G would lead to unstable states. In that sense, these are the *optimal states*. In Fig. 2, we have also added the line at which the L-H transition power threshold $M = 1$ occurs. The states to the right of this line correspond to $M > 1$ and thus they are in the H-mode. Since we are using the confinement time scaling for the H-mode, the states lying to the left of the $M = 1$ line should be regarded as meaningless, and therefore, the optimal states for densities below the one for the crossing of the lines $M = 1$ and $P_{\mathrm{aux},i} = 0$ (in this case $n_e = 1.15\ n_{e0}$) are given by the line $M = 1$, since that would give the maximum attainable Q_G for a given P_{fusion}, as seen from Fig. 2. Returning to the example of the reference point (1, 1), we note that when moving along the isoline of $P_{\mathrm{fusion}} = 489$ to increase the gain, the $M = 1$ line is crossed before reaching the $P_{\mathrm{aux},i} = 0$ line, and thus the maximum gain is limited to $Q_G \approx 13$.

In Fig. 3, we show the POPCON plots of the helium ash fraction, $f_\alpha = n_\alpha/n_e$. It can be concluded from Figs. 2 and 3 that increasing Q_G while keeping the fusion power constant implies increasing the helium ash fraction.

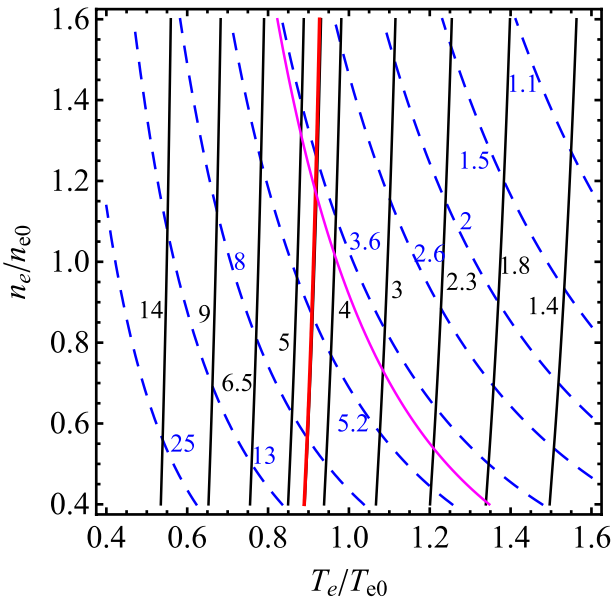

Fig. 4. Case f_{Be} and n_{Ar} constant with $H = 1$. Contours of $n_e\tau_E/10^{20}$ in seconds per cubic meter and the energy confinement time τ_E (dashed lines) in seconds. Red line: $P_{\mathrm{aux},i} = 0$. Magenta line: $M = 1$.

This is mainly a consequence of an increment in the energy confinement time of the helium ash, which we took proportional to τ_E.

Fig. 4 shows the contour plots of the Lawson parameter $n_e\tau_E$ (normalized to 10^{20} s/m^3) together with the plots of constant energy confinement time as obtained from the IPB98(y, 2) scaling. Here, we observe that the boundary line $P_{\mathrm{aux},i} = 0$ superposes almost perfectly with the line $n_e\tau_E = 4.5 \times 10^{20}$ s/m^3. This is thus a maximum value for

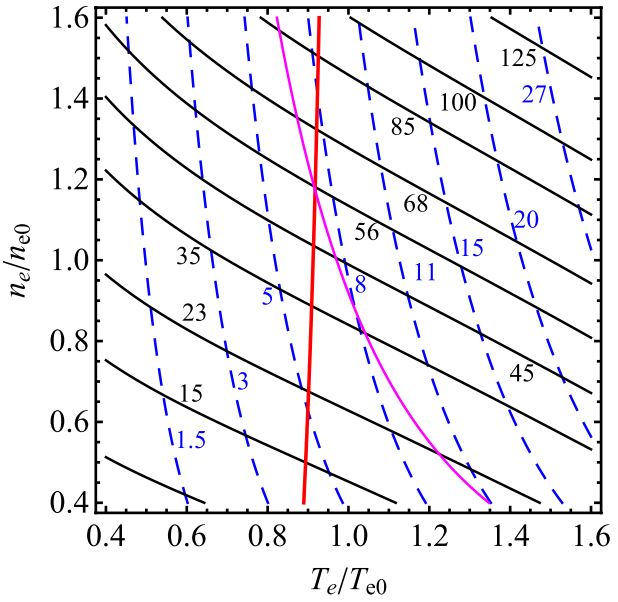

Fig. 5. Case f_{Be} and n_{Ar} constant with $H = 1$. Contours plots of the total radiated power, bremsstrahlung plus cyclotron, and just cyclotron radiation (dashed lines) in megawatts, together with $P_{aux,i} = 0$ (red line) and $M = 1$ (magenta line).

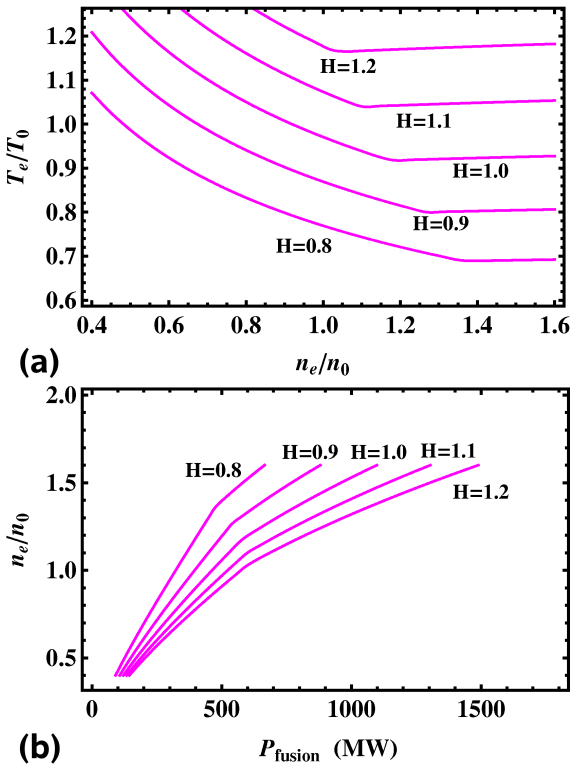

Fig. 6. Optimal operation points for confinement enhancement factors $H = 0.8, 0.9, 1, 1.1$, and 1.2 in (a) space n_e versus T_e and (b) n_e versus P_{fusion} plane, when f_{Be} and n_{Ar} are constant.

the Lawson parameter since states to the left of this line are not attainable. We also observe that the line corresponding to the L-H transition threshold power $M = 1$ is similar to the neighboring τ_E contour lines and only lines with $\tau_E < 5$ s fall to the right of the $M = 1$ line. Thus, we can say that the requirement for H-mode operation sets a limit on the maximum confinement time, which for the present situation is $\tau_E \approx 5$ s.

In Fig. 5, we show the contour plots of the total radiated power, i.e., bremsstrahlung plus cyclotron, together with the contour lines of the cyclotron radiated power, and the strong temperature dependence of the cyclotron radiation.

The results shown in Figs. 1–5 correspond to a confinement time enhancement factor of $H = 1$. We also performed the same calculations using several values of H in the range $0.8 \leq H \leq 1.2$ with the same conclusion: the optimal operating burn regimes for a given fusion power, that is, those that maximize the gain Q_G, are also those for which $P_{aux,i} = 0$ or $M = 1$, whatever occurs first when T_e is reduced.

The influence of the H factor can be appreciated when considering only the optimal operation points that yield the maximum energy gain Q_G. In Fig. 6(a), we show the optimal states for several values of H ranging from 0.8 to 1.2 in a T_e–n_e plot. They are formed by the piecewise composition of the lines $P_{aux,i} = 0$ and $M = 1$, as mentioned above. As expected, the optimal temperature increases with H. In Fig. 6(b), the optimal density values are shown as a function of the total fusion power. It is seen that for a confinement enhancement factor $H = 1.2$, the fusion power can be as high as 1500 MW for densities around $n_e \sim 1.6 n_{e0}$, while at a low density, $n_e \sim 0.4 n_{e0}$, the fusion power produced is of the order of 100 MW for all H values.

The maximum energy gain attainable for a given P_{fusion} is shown in Fig. 7(a). This plot can be used in combination with those in Fig. 6 to determine the required density and temperature for a certain value of P_{fusion} for an optimal operation, and then obtain the corresponding value for the associated optimal energy gain. Alternatively, one could determine the plasma density and electron temperature for a given enhancement factor H from Fig. 6(a) and obtain the values of P_{fusion} and the optimal Q_G from Fig. 7.

A typical situation when operating a reactor would be to specify the desired P_{fusion} and the associated maximal Q_G and then determine the required plasma parameters n_e and T_e at which the machine should operate. In order to automate this task, we could obtain a practical expression to be used to find n_e and T_e when a certain value of Q_G is given for optimal conditions. This is done with a polynomial fit to the values obtained from the solutions of the equations in terms of Q_G and H. The polynomial functions $n_e(Q_G, H)$ and $T_e(Q_G, H)$ provide good agreement with the sixth- and fourth-degree polynomials in Q_G and H, as it can be seen in Fig. 8, where the computed points and the analytical fits are shown for both functions. The functions $n_e(Q_G, H)$ and $T_e(Q_G, H)$ can then be used to obtain the optimal operating state n_e and T_e once Q_G and H are specified.

Another possible application of functions $n_e(Q_G, H)$ and $T_e(Q_G, H)$ occurs in a load-following operation in which it is desired to modify the total fusion power to a higher or a lower value to satisfy energy supply demands, in such a way that not only the initial and final operating points are optimal but also all the transient states. Thus, if we are initially in an optimal state for a given enhancement factor H for

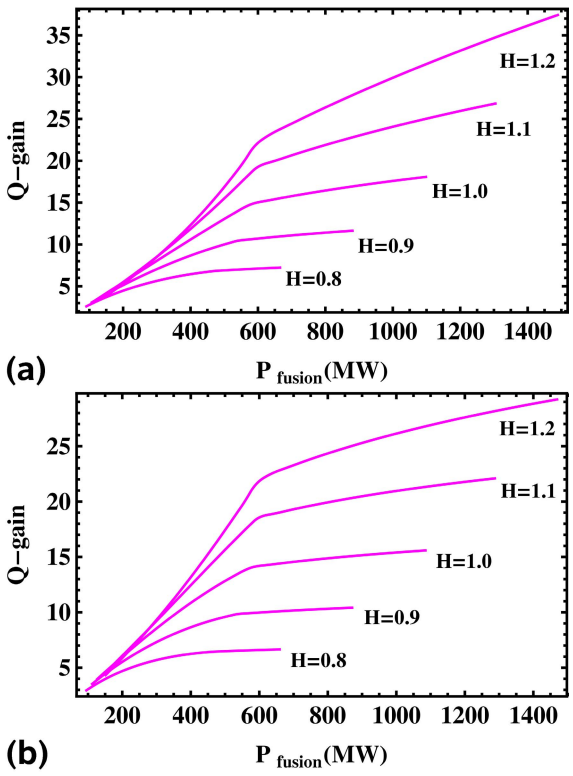

Fig. 7. Energy gain Q_G as a function of P_{fusion} at the optimal operation points for confinement enhancement factors $H = 0.8, 0.9, 1, 1.1$, and 1.2. (a) Case f_{Be} and n_{Ar} constant (Section III-A). (b) Case f_{Be} and f_{Ar} constant (Section III-B).

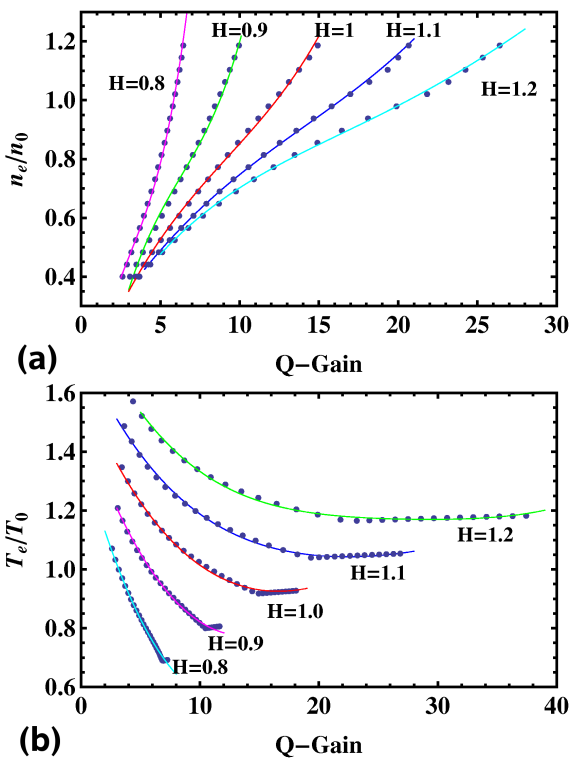

Fig. 8. Case f_{Be} and n_{Ar} constant. Polynomial fit in Q and H for the optimal operational points computed from the dynamical equations for (a) density and (b) temperature showing good agreement when n_e is of sixth order and T_e is of fourth order.

the confinement of the system, we can move along the corresponding boundary line $(P_{\text{aux},i} = 0)/(M = 1)$ given in Fig. 6(a) starting from the initial operating density until the operating density corresponding to the desired fusion power has been reached, as given in Fig. 6(b).

B. Case f_{Be} and f_{Ar} Constant

Argon is an impurity that can be externally controlled, so one can choose to maintain its fraction f_{Ar} fixed instead of holding a constant density n_{Ar} as before. Beryllium content is not controlled from the outside since it comes from the walls, so we still keep f_{Be} constant. The Ar fraction is fixed to the reference value $f_{\text{Ar}} = 0.0012$. When this is done, there are some differences from the results of the previous section. The most important is that the maximum energy gain Q_G is lower, as it can be seen in Fig. 7(b) where Q_G as a function of the fusion power is shown for $f_{\text{Ar}} =$ constant, compared with the case of $n_{\text{Ar}} =$ constant in Fig. 7(a). This is due to the fact that the Ar impurity density increases as the electron density rises, which is when the energy gain would be maximized. Thus, the larger radiative losses have to be compensated by auxiliary heating to the electrons, which diminishes Q_G.

The POPCON diagrams for the case $H = 1$ are similar to those in Figs. 1–5. There is also a boundary line for $P_{\text{aux},i} = 0$ at almost the same position. In Fig. 9, the contour plots of Q_G and P_{fusion} are shown for comparison. The auxiliary power needs are opposite for electrons and ions if the same (n_e, T_e) state for $n_{\text{Ar}} =$ constant is to be kept: for densities larger (smaller) than the nominal n_{e0}, $P_{\text{aux},e}$ has to be increased (decreased), while $P_{\text{aux},i}$ has to be slightly reduced (raised). The largest possible confinement time for the attainment of an H-mode is almost the same as in the case of constant Ar particle density, i.e., $\tau_E < 5$ s. Similarly the limit value for the Lawson parameter is almost the same as before, $n_e\tau_E/10^{20}$ s/m^3 < 4.5, and the coincidence of the $n_e\tau_E =$ constant line with the boundary $P_{\text{aux},i} = 0$ is as good as in the constant n_{Ar} case.

The cyclotron radiation power is the same in both cases; however, when the electron density increases, the bremsstrahlung and line radiation are larger in the case of constant f_{Ar}, thus increasing the total power radiated, and hence, the total auxiliary heating power must increase for larger electron densities and, conversely, for smaller electron densities, it diminishes. This effect is reflected in the gain Q_G, which for $f_{\text{Ar}} =$ constant is smaller than for $n_{\text{Ar}} =$ constant when $n_e > n_{e0}$ and larger when $n_e < n_{e0}$, as seen in Fig. 9.

C. Case With No Impurities

The ideal situation in which the reactor operates with no impurities, although hardly achievable in practice, has interest as a reference situation. For this reason, we included this case in our study as an ideal state to compare with. In Fig. 10, we show the POPCON plots for $H = 1$ corresponding to the auxiliary heating powers to electrons and ions, while Fig. 11

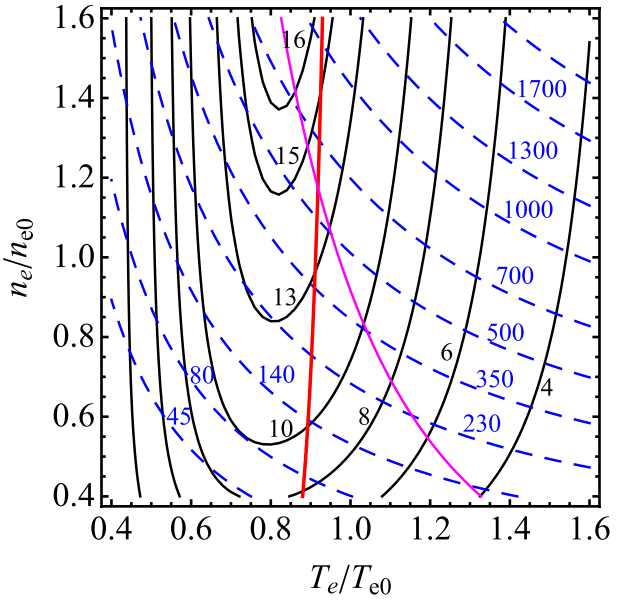

Fig. 9. Case f_{Be} and f_{Ar} constant with $H = 1$. Contour plot for the total fusion power in megawatts (dashed lines) and the Q-gain factor (solid lines), together with lines for which $P_{\mathrm{aux},i} = 0$ (red line) and $M = 1$ (magenta line).

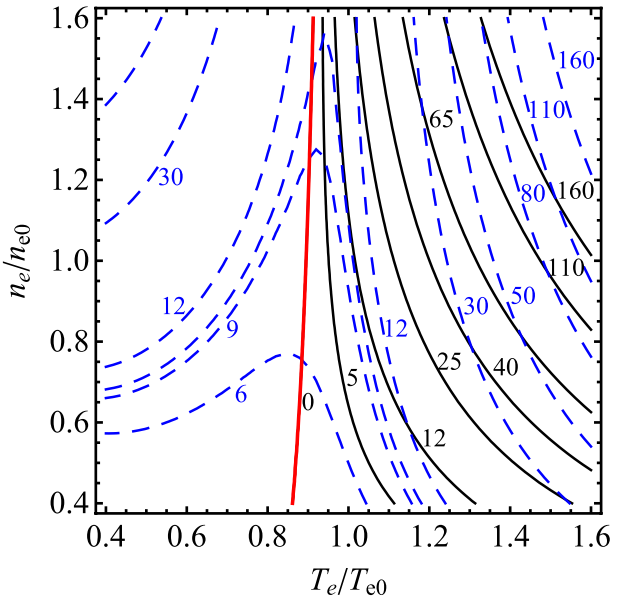

Fig. 10. Case with no impurities and $H = 1$. Contour plot of the auxiliary heating power to electrons (dashed lines) and the ions (solid lines) in megawatts. Red line: $P_{\mathrm{aux},i} = 0$.

shows the contour plots for the gain Q_G and the total fusion power. Qualitatively, these and the other contour plots look similar to those with impurities. However, due to the smaller Z_{eff} value, the bremsstrahlung and line radiation losses are much smaller in the system that contains no impurities, and hence, the fusion gain here is significantly larger than in the previous cases where impurities are present. This can be seen by comparing Fig. 11 with Figs. 2 and 9. This is because the quasi-neutrality condition for a given n_e value gives a higher DT fuel density when no impurities are present, and hence, the fusion power is higher.

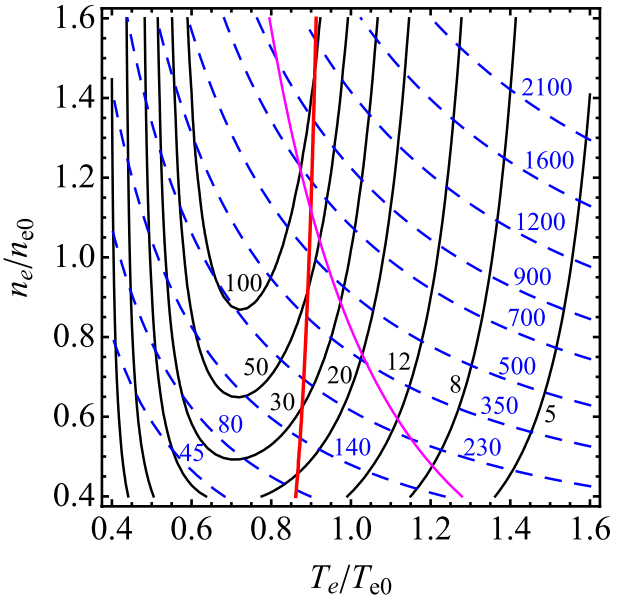

Fig. 11. Case with no impurities and $H = 1$. Contour plot of the total fusion power in megawatts (dashed lines) together with the Q-gain factor (solid lines). Red line: $P_{\mathrm{aux},i} = 0$. Magenta line: $M = 1$.

An interesting feature when impurities are absent is that the contour curves for $P_{\mathrm{aux},e}$ have a turning point in density at high n_e within the allowed region (i.e., $P_{\mathrm{aux},i} > 0$ and $M > 1$), very close to the boundary line. This means there are two possible states with the same $P_{\mathrm{aux},e}$ and P_{fusion} values, each having different gain factors Q_G. Therefore, a higher energy gain could be achieved without necessarily decreasing the auxiliary power to electrons and corresponds to an operating state with a lower temperature. This is due to the fact that when lowering the electron temperature and impurities are not present, there is only a moderate increase in ohmic heating power entering (17), which is then dominated by a faster decrease in the ion auxiliary power. An analogous effect does not occur in the presence of impurities because one of the corresponding operating states with the same $P_{\mathrm{aux},e}$ value falls within the inaccessible region $P_{\mathrm{aux},i} < 0$. It is worth mentioning that even in complete absence of impurities, there are no allowed states with total $P_{\mathrm{aux}} = 0$ and thus an ignited state is not possible for the ITER-like plasma parameters used in this paper.

Note that the boundary line $P_{\mathrm{aux},i} = 0$ is almost unaffected by the presence of impurities owing to the fixed ion loss rate assumed. On the other hand, impurities have the effect of reducing the region of states operating in the H-mode, since the L-H threshold line $M = 1$ moves to the right with respect to the case with no impurities.

D. Effect of Variation of Electron/Ion Relationships

In the computations so far, it has been assumed that $T_i/T_e =$ constant and $\tau_{E,i} = \tau_{E,e}$, which will not necessarily apply in actual operating conditions. In order to explore how much these restrictions affect the results, we have analyzed some cases changing the relations. It is convenient to mention that in our approach, T_i has to be obtained from a relationship

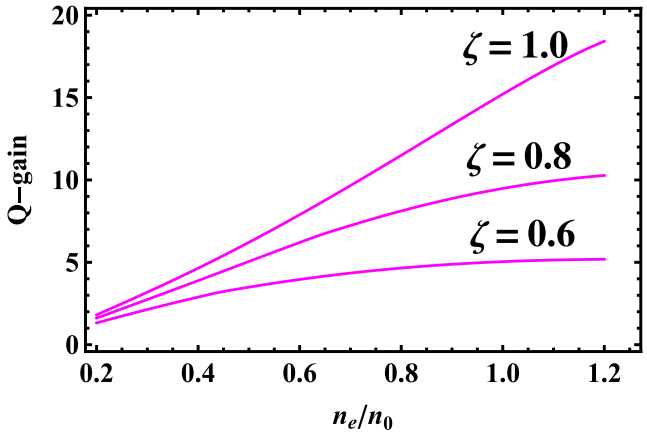

Fig. 12. Q-gain factor as a function of density for three values of $\zeta = \tau_{E,i}/\tau_{E,e}$, when $H = 1$.

with T_e in order to be able to represent the reactor states in the two-variable space T_e–n_e. In the first modification, we considered a case in which the temperature difference T_e–T_i is kept constant instead of the ratio T_i/T_e. The results obtained are qualitatively the same, but the contours are slightly modified.

In order to have different energy transport rates for ions and electrons, which is more adequate for $T_e \neq T_i$, we took $\tau_{E,i} = \zeta\tau_{E,e} = \zeta\tau_E$ so that the scaling law is the same. When $\zeta < 1$, the reduced ion energy confinement substantially reduces the energy gain. Fig. 12 shows the Q_G values as a function of density for three values of ζ, evidencing the large reduction in fusion gain, especially at large densities: there can be a fourfold reduction when $\tau_{E,i}$ decreases by 60%.

IV. Discussion and Conclusion

Using a 0-D two-temperature model, we have analyzed the different operating conditions in a tokamak fusion power plant with ITER-like parameters. Operational states are characterized by their density and electron temperature and are presented using POPCON plots in the T_e–n_e space. Consequently, the ion temperature has to be given in terms of T_e, either as a rational relation (T_i/T_e = constant) or a difference relation ($T_e - T_i$ = constant). These relationships can be kept by externally controlling ion and electron auxiliary heating. The operating states of the system can then be represented in a pictorial way, allowing straightforward analysis and interpretation. We considered the impurities solely consisting of a light component, Be, and a heavy component, Ar. While the Beryllium fractional density was always assumed constant, the cases with fixed number density of Ar and fixed fractional density n_{Ar}/n_e were analyzed, and only minor differences were found.

An important result is that irrespective of the impurity concentration, the optimal burn regimes (the operating conditions that maximize the Q-gain for a given fusion power level) are obtained when the auxiliary heating power to the plasma ions is zero, while staying in the H-mode. This means that a possible way to increase the power gain without changing the fusion power would be to shut off the source of auxiliary power to ions (e.g., neutral beam injection (NBI) or ion cyclotron resonance heating (ICRH)), provided that T_i decreases in the same proportion as T_e does. For this to happen, an appropriate refueling should be implemented to increase n_e in the right amount. This may be an attractive way to optimize the operation of a power plant maintaining the same fusion power. Another way to hold T_i/T_e fixed would be through an alpha channeling process in which some portion of the alpha particle energy is captured by waves and delivered to the ions [27]. This could even produce a hot ion mode in extreme conditions; however, this regime cannot be described by our model.

For the operation at the optimal states, we analyzed the effect of changing the value of the energy confinement time enhancement factor H in the IPB98(y, 2) scaling, showing improved fusion conditions at higher H as expected. Optimal operating curves were found for the plasma parameters and the Q-gain as a function of P_{fusion}, which provide the values needed for optimal operation at a given fusion power; these could be used to asses the plausibility of reaching a given optimal state. It is proposed that a fusion reactor could operate in load-following mode maintaining optimal conditions, by controlling the density [Fig. 6(b)] through DT fueling.

The operation of the reactor in a given optimal state could be maintained using a control system that adjusts the refueling rate and the external auxiliary heating when a fluctuation in the plasma parameters is detected. A possible control system based on an artificial neural network has been previously developed [29].

The results reported for the case T_i/T_e = constant were reproduced when the alternative condition $T_e - T_i$ = constant is used, qualitatively obtaining the same behavior. This indicates that the results are not very much dependent on the kind of relation used to obtain the ion temperature at the operating points, and therefore, our qualitative results apply quite generally in the operation of the fusion reactor. When the electron and ion energy confinement times are allowed to differ (since the assumed constraint $\tau_{E,i} = \tau_{E,e}$ may not be completely consistent with a two-temperature plasma), with $\tau_{E,i} < \tau_{E,e}$, the fusion performance is considerably degraded. This means that the performance values obtained here should be regarded as upper bounds.

As an exercise of how much the operation of a fusion reactor might improve were it possible to get rid of the impurities, we considered operation with a clean plasma. While most qualitative results still hold, the performance greatly improves having increments >20% for P_{fusion} and threefold in Q_G. It is also possible to have a bifurcation where two states with the same $P_{\mathrm{aux},e}$ and n_e have different burning conditions. Although this may prove useful for a more versatile operation of a reactor, it remains elusive until cleaner plasmas can be produced.

Acknowledgment

The authors would like to thank P. G. de la Parra for providing assistance in the computations of Section III-D.

References

[1] E. Rebhan, U. Vieth, D. Reiter, and G. H. Wolf, "Effect of helium concentration on ignition curves with energy confinement time including radiation losses," *Nucl. Fusion*, vol. 36, no. 2, p. 264, 1996.

[2] E. Rebhan and U. Vieth, "Burn stability and a safe operating regime of a tokamak reactor with ITER scaling," *Nucl. Fusion*, vol. 37, no. 2, p. 251, 1997.
[3] A. V. Eremin and A. A. Shishkin, "Particle and power balance in fusion plasma with different fuelling scenarios and helium ash removal," *Eur. Phys. J. D*, vol. 54, no. 2, pp. 503–509, 2009.
[4] O. Mitarai and K. Muraoka, "Ignition analyses with ITER89P and ITER93HP scalings for burn control and diagnostics in ITER-ID," *Plasma Phys. Controlled Fusion*, vol. 40, no. 7, p. 1349, 1998.
[5] O. Mitarai and K. Muraoka, "Ignition analysis for burn control and diagnostic developments in ITER," *Nucl. Fusion*, vol. 37, no. 11, p. 1523, 1997.
[6] M. Shimada *et al.*, "Progress in the ITER physics basis: Overview and summary," *Nucl. Fusion*, vol. 47, no. 6, p. S1, Jun. 2007.
[7] W. A. Houlberg, S. E. Attenberger, and L. M. Hively, "Contour analysis of fusion reactor plasma performance," *Nucl. Fusion*, vol. 22, no. 7, p. 935, 1982.
[8] J. J. Martinell, "Optimization and thermal stability studies of Ignitor and ITER," *Radiat. Effects Defects Solids, Incorp. Plasma Sci. Plasma Technol.*, vol. 166, no. 10, pp. 821–828, 2011.
[9] J. J. Martinell and J. E. Vitela, "Thermal stability studies of an experimental nuclear fusion reactor," *J. Phys., Conf. Ser.*, vol. 511, no. 1, p. 012043, 2014.
[10] J. J. Martinell and C. Gutiérrez-Tapia, "Induction of poloidal rotation by a radial ponderomotive force of electron cyclotron waves," *Phys. Plasmas*, vol. 8, no. 6, p. 2808, 2001.
[11] R. J. Goldston and P. H. Rutherford, *Introduction to Plasma Physics*. Bristol, U.K.: IOP, 1995.
[12] F. Albajar, M. Bornatici, and F. Engelmann, "RAYTEC: A new code for electron cyclotron radiative transport modelling of fusion plasmas," *Nucl. Fusion*, vol. 49, no. 11, p. 115017, 2009.
[13] S. P. Hirshman and D. J. Sigmar, "Neoclassical transport of impurities in tokamak plasmas," *Nucl. Fusion*, vol. 21, no. 9, p. 1079, 1981.
[14] H.-S. Bosch and G. M. Hale, "Improved formulas for fusion cross-sections and thermal reactivities," *Nucl. Fusion*, vol. 32, no. 4, pp. 611–631, 1992.
[15] M. Shimada *et al.*, "Physics design of ITER-FEAT," *J. Plasma Fusion Res. Ser.*, vol. 3, pp. 77–83, 2000.
[16] L. Spitzer, Jr., *Physics of Fully Ionized Gases*, 2nd ed. New York, NY, USA: Wiley, 1962.
[17] E. Asp *et al.*, "JETTO simulations of T_e/T_i effects on plasma confinement," *Plasma Phys. Controlled Fusion*, vol. 47, no. 3, p. 505, 2005.
[18] T. C. Luce, C. C. Petty, and J. G. Cordey, "Application of dimensionless parameter scaling techniques to the design and interpretation of magnetic fusion experiments," *Plasma Phys. Controlled Fusion*, vol. 50, no. 4, p. 043001, 2008.
[19] Y. R. Martin and T. Takizuka, "Power requirement for accessing the H-mode in ITER," *J. Phys., Conf. Ser.*, vol. 123, no. 1, p. 012033, 2008.
[20] R. Aymar, P. Barabaschi, and Y. Shimomura, "The ITER design," *Plasma Phys. Controlled Fusion*, vol. 44, no. 5, pp. 519–565, 2002.
[21] M. Greenwald *et al.*, "A new look at density limits in tokamaks," *Nucl. Fusion*, vol. 28, no. 12, p. 2199, 1998.
[22] M. Greenwald, "Density limits in toroidal plasmas," *Plasma Phys. Controlled Fusion*, vol. 44, no. 8, p. R27, 2002.
[23] M. Z. Tokar, "On Greenwald density limit in H-mode," *Phys. Plasmas*, vol. 16, no. 2, p. 020704, 2009.
[24] J. E. Vitela and M. Coronado, "Fluctuations of a charged Brownian particle in a plasma," *Phys. Rev. A*, vol. 42, no. 4, p. 2354, 1990.
[25] J. Wesson, *Tokamaks*. Oxford, U.K.: Clarendon, 2004.
[26] T. H. Stix, "Heating of toroidal plasmas by neutral injection," *Plasma Phys.*, vol. 14, no. 4, p. 367, 1972.
[27] N. J. Fisch, "Elementary processes underlying alpha channeling in tokamaks," in *Proc. AIP Conf.*, vol. 1478. 2012, p. 80.
[28] N. J. Fisch and J.-M. Rax, "Interaction of energetic alpha particles with intense lower hybrid waves," *Phys. Rev. Lett.*, vol. 69, no. 4, p. 612, 1992.
[29] J. E. Vitela and J. J. Martinell, "Burn conditions stabilization with artificial neural networks of subignited thermonuclear reactors with scaling law uncertainties," *Plasma Phys. Controlled Fusion*, vol. 43, no. 2, p. 99, 2001.

Authors' photographs and biographies not available at the time of publication.